EPSC Abstracts
Vol. 12, EPSC2018-871, 2018
European Planetary Science Congress 2018

Impact-Induced Melting by Giant Collision Events

L. Manske[1,2], K. Wünnemann[1,2], M. Nakajima[3], C. Burger[4] and A.-C. Plesa[5], [1]Museum für Naturkunde, Leibniz Institut for Evolution and Biodiversity Science, 10115 Berlin, Germany, lukas.manske@mfn-berlin.de, [2]Institute for Geological Sciences, Planetary Sciences and Remote Sensing, Freie Universität 12249 Berlin, Germany [3]Department of Terrestrial Magnetism, Carnegie Institution for Science Washington, DC 20005, USA, [4]Department of Astrophysics, University of Vienna, 1180 Vienna, Austria. [5]German Aerospace Center (DLR), 12489 Berlin, Germany.

1. Introduction

We revisited the long-standing problem of the generation of melt as a consequence of giant impact events, which may not be accurately addressed by classical scaling-laws [1,2]. During the accretion phase, the thermochemical evolution of the terrestrial planets was heavily influenced by giant collisions with other cosmic bodies such as the Moon-forming event on the young Earth [3]. Besides variations in the compositional budged, such impacts transfer a significant amount of energy to heat up the planet and cause the formation of local magma ponds or even global magma oceans. For smaller impact events (smaller than basin-forming), the amount of impact-induced melting can be predicted by scaling-laws [1,2]. But on a larger scale they might not be accurate as they do not account for the initial temperature or lithostatic pressure of planets interior, especially where the initial temperatures are close to the solidus (especially for younger planet). To better understand and quantify the mechanism of heat production and melting during large-scale impact events we conducted a series of numerical models and determined the volume of melt production.

2. Methods

We use the iSALE Eulerian shock physics code [4,5] (Version *Dellen*) and two different Smooth-Particle-Hydrocodes (SPH) [6,7] to model large-scale hypervelocity impact events. The thermodynamic state (EoS) is calculated by ANEOS [8] for basalt, dunite, and iron representing the planetary crust, mantle and core, respectively.

To locate and quantify the volume of the impact-induced melt we measure the material's (post-impact) final temperature (or entropy) T_f and compare it with the pressure-dependent melt temperature [9] (or entropy) for incipient T_{M1} and complete melting T_{M2}. To bypass diffusion-based inaccuracies of the temperature field calculated by iSALE, we use massless Lagrangian tracers to record the material's highest shock pressure P_{peak} (peak shock pressure), which is proportional to the raise of the temperature [2]: $P_{peak} \propto \Delta T$. Using ANEOS, the temperature increase ΔT is then worked out via the thermodynamic release path from the peak shock pressure P_{Peak} state to the final (post-impact) pressure P_f state and can be added to the initial temperature T_{Ini} to derive the final temperature $T_f = \Delta T + T_{Ini}$. It should be noted, that ΔT is not only a function of the peak shock and final pressure, but also of the initial pressure and temperature P_{Ini}, T_{Ini} conditions. The final temperature (or entropy) T_f can then be compared to the melt temperatures (or entropies) $T_{M1,2}(P_f)$ to determine whether the material is (partially) molten or not. Tracers also record the material's displacement, which allows for taking decompression melting into account. Decompression is a consequence of the stratigraphic uplift of the material in the course of crater formation resulting in a lower lithostatic pressure and hence lower melting temperatures $T_{M1,2}(P_f)$ than before impact $T_{M1,2}(P_{Ini})$. To measure the influence of decompression melting, we compare the temperature increase caused by the shock ΔT with the change of the melt temperature caused by the stratigraphic uplift: $\Delta T_M = T_{M1,2}(P_f) - T_{M1,2}(P_{Ini})$ (cf. Fig. 2, left).

We carried out a series of numerical models for Mars and the Earth's Moon assuming individual initial composition and temperature distributions, impact velocities, and gravity. While neglecting differentiated bodies at this stage, the projectiles consists of a dunitic composition and their radii were resolved by 50 cells (50 CPPR) in all iSALE models. In the SPH models we used about 1 million particles. The initial thermal profiles ($T_i = f(P)$) differ from hot to cold setups, representing earlier to more recent stages of the planets' thermal evolution, respectively [10].

3. Results

In each model series we choose an initial temperature T_{Ini} (planet's age) and vary the impactor diameter L and velocity v_i. We calculate reference models, which are based on simplified assumptions corresponding to the scaling-laws but with a planet-like layered target. These models match the scaling-laws well, while they indicate a crust or mantle melt regime depending on penetration depth (L,v_i) and planet structure (cf. Fig. 1).

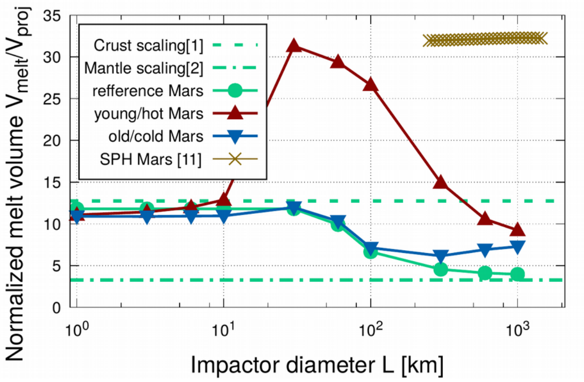

Fig. 1. : Normalized melt production for Mars-like parameters with v_i = 15km/s. Scaling laws [1,2] compared to a reference model (green). More realistic models based on temperature profiles corresponding to different ages after planet formation (red: 40 Myr/ blue: 4500 Myr) [10] are shown by triangles. Preliminary SPH code simulations are presented in ocher [11].

Fig. 1 indicates, that the more realistic models (triangles) are approximately in agreement with classic scaling for smaller impacts; however, larger events are not. In particular, the normalized melt production ($V_{melt}/V_{projectile}$) shows large variations that are caused by the depth dependent distribution of the initial temperature T_i and thus the evolutionary state of the planet. This leads to a depth dependence of the threshold temperature increase to cause melting $\Delta T_{Melt}(z) = \Delta T_{M1,2}(P(z)) - \Delta T_{Ini}(z)$. It can be shown that the maximum normalized melt production occurs at impactor sizes, where the main melt body is located in the area, which requires the lowest ΔT_{Melt}. This area is often located at the bottom of the lithosphere.

For even bigger impactor sizes, SPH code simulations have been added [11] (ocher crosses). Those simulations are based on a temperature profile, where T_i is equal to the solidus T_{M1}. This relation also holds true for a certain depth range of the young Mars model. Using a impactor diameter of L = 30 km, most of the melt is produced in this range, which makes the normalized melt volumes comparable to the SPH model. One can see, that the differently derived melt volumes are almost equal in this case.

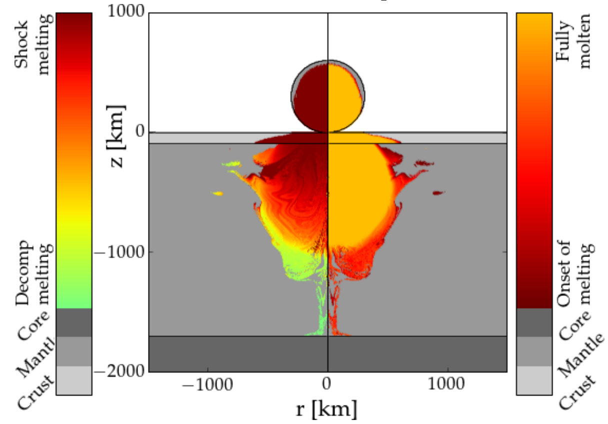

Fig. 2.: Melt distribution mapped back to the initial Position. Colors indicate molten material. Left: Influence of decompression melting. Right: Degree of partial melt.

Fig. 2 implies, that the more the material can rise and the closer the temperature and melt temperatures are, the more decompression melting contribute to melt production. Thus decompression melting is sensitive to the chosen initial temperature T_i, melt temperature $T_{M1,2}$ and impactor.

Our goal is to derive a lookup table for impact-induced melt volumes V_m as a function of impact parameters $V_m = f(L, v_i, T_i, P_f)$ based on merged SPH and mesh based simulations.

Acknowledgements

We gratefully acknowledge the developers of iSALE, including Gareth Collins, Dirk Elbeshauesn, Boris Ivanov and Jay Melosh. This work was funded by the Deutsche Forschungsgemeinschaft (SFB-TRR 170, Subproj. C2, C4).

References

[1] Abramov O. et al. (2012) Icarus 218, 906-916. [2] Pierazzo et al. (1997) Icarus 127, 408-423, 1997. [3] Marchi S. et al. (2014) Nature 511, 578-582. [4] Collins. G. S. et al. (2004) MPS. 39, 217-231. [5] Wünnemann K. et al. (2006) Icarus 180, 514–527. [6] Schäfer C. et al., (2016) Astronomy & Astrophysics 590, A19. [7] Nakajima & Stevenson, (2015) EPSL 427, 286-295. [8] Thompson and Lauson (1972) Report SC-RR-71 0714, Sandia Natailonal Lab. [9] Ruedas, T. and Breuer, D. (2017) JGR, 122, 1554-1579 [10] Plesa, A.-C. et al. (2016) JGR 121, 2386-2403. [11] Nakajima et al. (2016) AGU, P51A-2118.